# Determination of the effective density and fractal dimension of PM emissions from an aircraft auxiliary power unit

Emamode A. Ubogu, James Cronly*, Bhupendra Khandelwal, Swapneel Roy

*Low Carbon Combustion Centre, University of Sheffield, Unit 2, Crown Works Industrial Estate, Rotherham Road, Sheffield S20 1AH, United Kingdom*

## ARTICLE INFO

## ABSTRACT

Gas turbine particulate matter (PM) emissions contribute to air quality degradation and are dangerous to both human health and the environment. Currently, PM mass concentrations determined from gravimetric measurements are the default parameter for gas turbine emissions compliance with PM regulations. The measurement of particle size however, is of significant interest due to its specific effects on health and climate science. The mass concentration can be determined from the number-size distribution measurement but requires the experimental evaluation of effective density of a number of particles to establish the power-law relationship. In this study, the effective density of PM emissions from an aircraft Auxiliary Power Unit (APU) with petroleum diesel, conventional aviation fuel (Jet A-1) and a multicomponent surrogate fuel (Banner NP 1014) as combusting fuels have been compared. An experimental configuration consisting of a Differential Mobility Analyzer, a Centrifugal Particle Mass Analyzer and a Condensation Particle Counter (DMA-CPMA-CPC) was deployed for this purpose. Overall, a decrease in the effective density (220–1900 $km^{-3}$) with an increase in the particle size was observed and found to depend on the engine operating condition and the type of fuel undergoing combustion. There was a change in the trend of the effective densities between the PM emissions generated from the fuels burnt and the engine operating conditions with increasing particle size.

## Introduction

The impact of particulate matter (PM) emissions on human health and the environment has led to increased emphasis of the effectiveness of emission measurement techniques from gas turbines. Typically, PM emissions are measured by mass and are presented as mass concentrations. In recent years however, the particle number-size distribution has received increased attention as a measurement metric due to the direct relationship of particle size with human health. Mathematically, the two parameters are linked and as such, number-size distribution measurement can be converted to mass concentration. In theory, the density of different particle sizes of the particles counted would be required. Despite this, researchers have often justified the assumptions of a unit density (Anderson et al., 2005; Kinsey et al., 2010, 2012; Lobo et al., 2011; Petzold et al., 2011) using the bulk density of carbon (1200–1900 kg/m³) (Corporan et al., 2008; Hagen et al., 1998) to calculate the particle mass concentrations.

Recognizing the fact that the gas turbine particle emissions are fractal aggregates with internal voids or agglomerates forming a complex fractal chain structure with much larger dimensions (Vander Wal et al., 2014), the assumption of a unit or

* Corresponding author. E-mail: jcronly1@sheffield.ac.uk (James Cronly).

bulk density is overly simplistic. This is evident as up to 50% and 35% overestimations (Kinsey et al., 2012; Onasch et al., 2009) and underestimations (Petzold et al., 2011) have been recorded when compared to a typical mass concentration measurement instruments. Kinsey et al. (2012) attributes these differences to the variation in the density of the single particles that make up the particle emissions against the uniform density implied by the assumptions. Kelly and McMurry (1992) noted that by assuming a uniform particle density, the chemical composition of the PM samples is simply ignored.

A better density evaluation that recognizes the particle structures would be to use the effective density of the particles. The effective density is a parameter derived from the combination of two particulate measurement techniques (DeCarlo et al., 2004). Using this approach, the effective density of soot agglomerates has been reported to decrease with increasing particle size. Also, using an experimentally derived effective density rather than a uniform density, reasonable agreement with gravimetric data (Li et al., 2014; Symonds et al., 2007) has been observed from the PM size distributions of motor vehicle emissions. The same methods can be adapted to gas turbine PM measurements where similar challenges of ultra-low PM mass emissions occur.

To determine the effective density distribution of a statistically significant number of particles, a measure of the density of a large number of single particles would be ideal. As an area of ongoing research, various concepts have been developed to determine the effective densities of a significant number of particle sizes in a particular sample. Frequently used concepts involve one of the following combinations: mobility size–aerodynamic size, mobility size–particle mass, or aerodynamic size–particle mass. Another frequently used concept is based on the ratio of the gravimetrically derived mass to mobility equivalent volume. This concept was used by Li-Jones et al. (2007) at idle conditions of a T700-GE-700 helicopter engine and Timko et al. (2010) at various engine conditions of a PW308 turbine engine using gravimetric filters and a Multi Angle Absorption Photometer (MAAP) respectively to evaluate the particulate masses and the particle volume calculated using a Scanning Mobility Particle Sizer (SMPS). An average effective density of 1000 kg/m$^3$ was observed for the T700-GE-700 while values ranging between 400 to 820 kg/m$^3$ were observed for the PW308 depending on the type of fuel used and the engine thrust.

The electrical mobility size – aerodynamic size relationship can be realized using an Aerosol Particle Sizer (APS) and Scanning Mobility Particle Sizer (SMPS) in parallel, or a Differential Mobility Analyzer (DMA) and multi stage impactor as incorporated in the newly developed Dekati Mass Monitor (DMM) for real time evaluation of the particle mass concentration. Combining an aerosol mass spectrometer (AMS) and a SMPS, Timko et al. (2010) also evaluated the effective density using the PW308 engine and reported a density range of 710–840 kg/m$^3$ which depended on the fuel type and engine thrust. Similarly, Onasch et al. (2009) deployed the same concept to investigate the densities of a CFM56-2-C1 at full throttle and reported an average density of 1000 kg/m$^3$.

With the development of a particle mass classifier, the concept of mobility size and particle mass has become an attractive concept. The technique introduced by McMurry et al. (2002) is implemented by combining a DMA upstream of either an Aerosol Particle Mass Analyzer (APMA by Kenomax) developed by

Ehara et al. (1996) or a Centrifugal Particle Mass Analyzer (CPMA by Cambustion) developed by Olfert and Collings (2005). The APMA and CPMA are instruments that use the mass/charge ratio to classify particles based on their mass. The idea of the concept is to classify the particles based on their sizes using a DMA and further classify them based on their mass using the APMA or CPMA, with a Condensation Particle Counter (CPC) or electrometer downstream acting as a detector. An alternative approach is to have the CPMA placed upstream of a modified fast particle analyzer like the DMS500 or EEPS. With these approaches, the mass mobility exponent, $D_{me}$, which is a measure of the fractal dimensions and relates the particle mass, $m$, to its mobility diameter, $d_m$, is determined. To achieve this, several size-mass classifications are performed to obtain a large enough data set to generate a power law function from which the mass mobility exponent can be established, as shown in Eq. (1):

$$m = C \times d_m^{D_{me}} \tag{1}$$

This relationship can be expressed to define the effective density, $\rho_{eff}$, as shown in Eq. (2) (Abegglen et al., 2015; Durdina et al., 2014; Johnson et al., 2015):

$$\rho_{eff} = \frac{6}{\pi} \times \frac{m}{d_m^3} = k \times d_m^{D_{me}-2} \tag{2}$$

where $C$ is a scaling constant, $k$ is the mass-mobility prefactor ($k = 6C/\pi$). With this approach, Durdina et al. (2014) reported a mean effective density within 10% of the unit density (1000 kg/m$^3$) for a commercial turbofan engine (CFM56-7B26/3) from an undiluted exhaust sample with a Nafion dryer placed upstream of the DMA-CPMA-CPC instrumentation. Using a CPMA and a modified DMS500, Johnson et al. (2015) reported a varied density of 600 to 1250 kg/m$^3$ for CFM56-5B4/2P, CFM56-7B26/3, and PW4000-100 gas turbines but noted that the largest variability was observed for the undiluted sample without a catalytic stripper; an indication that the relative amount of semi volatile material produced was engine thrust dependent.

Previous studies have focused on the main engine of civilian or military fleets. In this study, the DMA-CPMA-CPC technique is used to determine the effective density of the exhaust particles of an APU. A primary objective of this paper is to compare the effective density data trends of the APU PM emissions from different fuels and different operating power settings.

## 1. Experimental set-up and procedures

### 1.1. Fuels

The test fuels include a multicomponent surrogate fuel herein referred to as Banner Solvent (Banner NP1014), a petroleum aviation fuel (Jet A-1), and petroleum Diesel. Selected fuel properties are presented in Table 1. Data for Jet A-1 and Banner Solvent have been provided from laboratory measurement, while the diesel fuel properties were taken from EN590:2009 (Automotive Fuel Requirements, 2009) except where otherwise referenced. Banner Solvent contains no amount of sulfur and aromatic compared to Jet A-1 fuel. It only contains the following normal alkanes; nonane, decane, undecane, dodecane, tridecane and tetradecane.

**Table 1 – Selected fuel properties.**

| Property | Jet A-1 | Diesel | Banner NP 1014 |
|---|---|---|---|
| Density at 15°C (kg/m$^3$) | 802 | 820–845 | 792.2 |
| Aromatic content (vol.%) | 19.2 | 24.0 | 0 |
| H/C ratio (mol/mol) | 1.899 | 1.797 | 2.155 ± 0.02 |
| Viscosity[i] (cSt) | 3.420 | 2.000–4.500 | 3.259 |
| Sulphur content (Mg/kg) | 370 | ≤10 | 0.7 |

[1]Diesel Viscosity specified at 40°C while the Jet A-1 limit is specified at −20°C.

### 1.2. Gas turbine

The test engine is a GTCP85 series gas turbine manufactured by Garrett-AiResearch (now Honeywell). It is an integral bleed type engine that can be used to provide power and compressed air. It has a single-can combustor with two stage centrifugal compressor with a compression ratio of 5:1 and a single stage radial inflow turbine. The engine is rated to produce bleed air flow of 58 kg/min at 220°C exhaust gas temperature (EGT) and no shaft work, a maximum shaft work of 149.2 kW and a maximum exhaust gas temperature (EGT) of 621°C. Mounted on a test bench at the University of Sheffield's Low Carbon Combustion Centre, it provides an ideal test environment to evaluate the emissions characteristics of new gas turbine test fuels. The engine is instrumented to monitor and log key engine operating parameters, such as temperature, pressure, engine RPM and fuel flow rates, *etc.*

Two engine powers setting have been investigated using the fuel flow as an indicator of the engine power. Table 2 lists the nominal values for Exhaust Gas Temperature (EGT), and Fuel flow rate achieved for the engine power settings.

The engine power settings investigated are; no load (NL) which is the same as the engine idle condition and bleed load (BL) which means the bleed air extraction was open with no electric load on the engine. For the NL conditions, the three test fuels have been investigated while only Jet A-1 was burnt at the BL engine power setting which has been previously reported (Lobo et al., 2015; Khandelwal et al., 2013; Roy and Khandelwal, 2015) to produce the highest smoke number when burning Jet A-1 fuel for various bleed conditions. Fig. 1 shows a schematic of the sampling system used to transport the exhaust sample to the PM instruments.

### 1.3. Emissions measurement set-up

The sampling system adopted parts of the emission certification regulations in the "Society of Automotive Engineers, Aerospace Information Report 6241" (2013). A single probe with a nominal internal diameter of 14.1 mm was used to continuously extract

**Table 2 – Nominal APU operating conditions.**

| Operating conditions | EGT (°C) | Fuel flow rate (g/sec) | RPM |
|---|---|---|---|
| NL | 304.2 ± 1 | 18.7 ± 0.5 | 41,698 ± 50 |
| BL | 406.4 ± 0.8 | 24.7 ± 0.3 | 41,120 ± 17 |

the APU exhaust samples to the PM instruments. The probe was positioned parallel to the exhaust gas flow and approximately 0.5 m downstream of the engine exhaust nozzle to ensure that fresh and non-aged exhaust were extracted. Directly attached to the probe was a stainless-steel sampling line with a nominal internal diameter of 8 mm which ran 8 m from the probe to a two-way splitter from which the exhaust samples split thereby delivering samples to a Differential Mobility Spectrometer 500 (DMS) developed and manufactured by Cambustion Ltd. and a DMA-CPMA-CPC configuration. Models of the individual instrument of the DMA-CPMA-CPC system are as follows; Differential Mobility Analyzer (DMA: TSI, Model 3081, TSI Inc., St. Paul, USA)–Centrifugal Particle Mass Analyzer (CPMA: Cambustion Ltd., Cambridge, UK)–Condensation Particle Counter (CPC: TSI, Model 3775; TSI Inc., St. Paul, USA).

The exhaust through the 8-meter sample line directly connected to the probe was left undiluted but kept heated to 160°C including the two-way splitter. The connecting sample lines between the splitter and the instrument were 5 m in length. The connecting sample line that supplies the DMA-CPMA-CPC system was unheated and the exhaust sample undiluted as the sample was left to cool down to meet the instrument exhaust sample temperature requirement. The exhaust sample to the DMS500 was heated to 160°C and diluted by a ratio of 60:1 using zero grade nitrogen. Dilution was in two parts and controlled from the DMS500 software interface. Primary dilution (5:1) occurred at the point the exhaust sample moved from the splitter to the DMS500 heated sample line and a second dilution (12:1) occurred inside the DMS500 using a rotating disc diluter. While dilution ratios are likely to have an impact on PM morphology, the effects of varying dilution ratios were not investigated in this work.

A minimum of four particle mass distributions have been evaluated with the DMA-CPMA-CPC for each of the test points. In general, the mass distributions of the particle sizes evaluated were less than 400 nm. These values are verified by the particle size distributions results of the DMS500 in next section. The DMA was used to select monodisperse aerosol particles of a desired electrical mobility size from the exhaust sample which were further classified by the CPMA. The selected sizes ranged between 30 and 450 nm in diameter. Using the particle mass charge ratio, the CPMA generates a mass spectral density fitted with a log-normal distribution. The mode mass spectral density is selected as the particle mass of the DMA-classified particles. The duration for one DMA-CPMA-CPC scan is of average duration of 6 min but is dependent on the resolution of the scan and initial estimate of the mass of the DMA single particles transferred to the CPMA. The engine run for each test point after engine stabilization was a minimum of 24 min per condition.

## 2. Results and discussion

### 2.1. Particle size and number distribution

Fig. 2 shows the number density of the particle size distribution (PSD) of the gas turbine PM emissions from the combustion of the test fuels at each engine operating condition. In general, the PSD are bimodal for all four test points. This is an indication of the presence of nucleation mode and accumulation mode
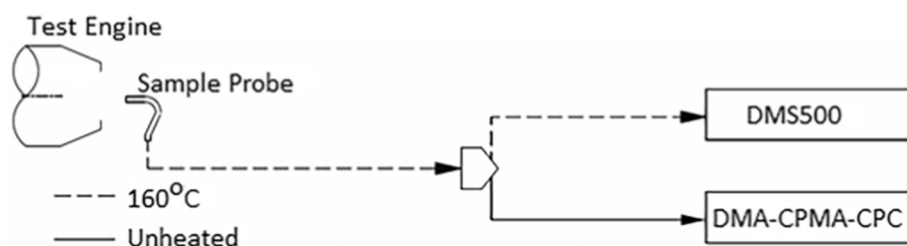
**Fig. 1 – Schematic of sampling system.**

represented by the first and second peak points respectively. The particle sizes range from approximately 5 nm to 500 nm for diesel and Jet A-1 at the NL engine power setting while the Banner Solvent particle sizes range from approximately 5 nm to 250 nm. The larger particles observed for Jet A-1 and diesel as compared to the Banner Solvent can be attributed to difference in the aromatic content in the fuels. As shown in Table 2, Banner Solvent has no aromatic content. The first peaks can be observed at approximately 31 nm for all the test points with Banner Solvent generated particles showing higher particle number concentration in nucleation mode compared to the diesel and Jet A-1 particles for the NL engine power setting. Banner Solvent nucleation mode particles can be considered organic carbon as the fuel contains no sulfur. The second peak is observable at 48, 64 and 86 nm for Banner Solvent, Jet A-1 and diesel respectively at the NL engine power setting. The accumulation mode particle size at the BL engine power setting are larger (86 nm) compared to the NL engine power setting (64 nm) as observed by comparing the Jet A-1 emissions at both engine power settings.

### 2.2. Particle effective density

Figs. 3 and 4 are plots of the effective density against the mobility diameter for the test fuels at the NL engine conditions and Jet A-1 at the NL and BL engine conditions respectively. Overall the

densities for the different particle sizes evaluated range between 220 and 1900 kg/m$^3$ and are observed to decrease with an increase in particle size. For example, the highest (200 nm) and lowest (30 nm) particle sizes evaluated for the Banner Solvent PM emission exhibit an effective density of 330 and 1900 kg/m$^3$, respectively.

While there is a general trend for the effective densities to decrease with increasing particle size, there are variations in density when varying the fuel type at specific sizes. Table 3 shows the effective densities of the mass scan of identical particle sizes for Banner Solvent and Diesel PM emissions.

For 150 and 200 nm particles sizes, lower effective densities can be observed for Banner Solvent compared to the Diesel generated PM emissions. In contrast, the effective density of the 30 nm diameter particles for the Banner Solvent PM emissions is higher. Similar trends can be observed for the Jet A-1 power law fit at the NL engine power setting compared to the Banner Solvent and Diesel PM emissions. The same effective density is predicted for a 30-nm particle diameter for both Jet A-1 and Diesel generated PM emission at the NL engine power setting. However, above 30 nm the Jet A-1 particle densities are higher and below which Diesel particle densities become higher.

The equations of the power law fit for the plots in Figs. 3 and 4 are detailed in Table 4. Matching the equations with Eq. (2), similar fractal dimensions obtained by Park et al. (2004) for a diesel and gas turbine engine at different engine loads can be
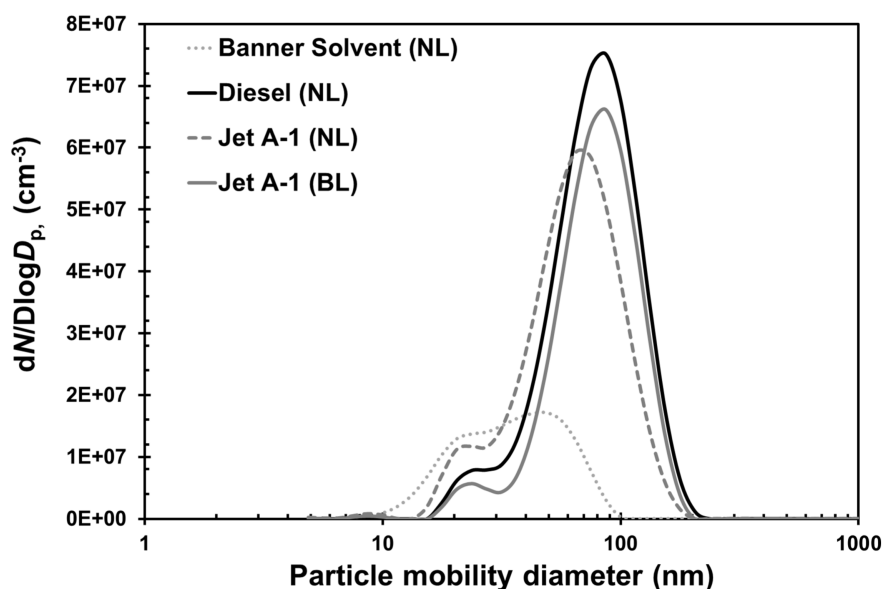


**Fig. 2 – Total PM number size distribution measured with DMS 500. PM: particulate matter.**
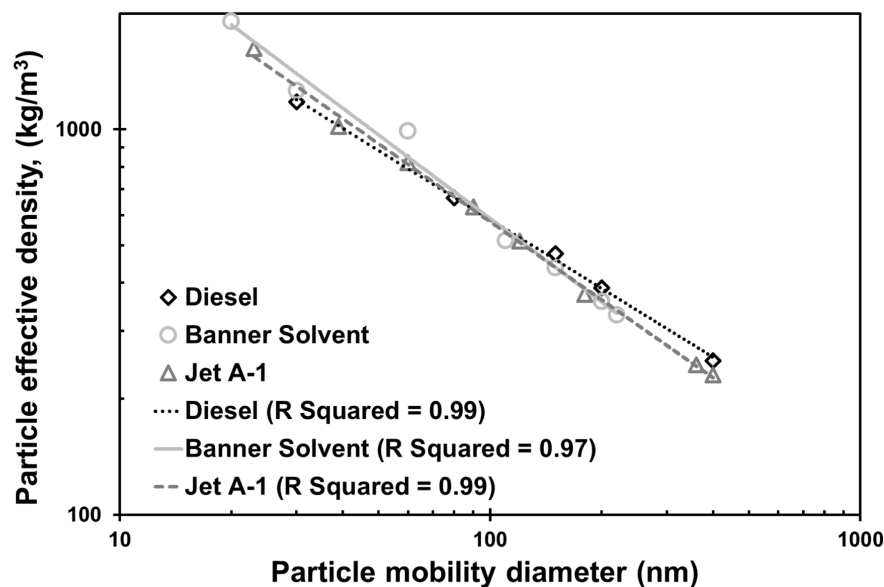
**Fig. 3 – Power law trend lines of effective densities against the mobility diameter for the test fuels at the NL conditions. NL: no load.**

observed. The fractal dimension is important as it helps to understand the structural geometry of the PM emissions. Banner Solvent generated PM emission shows the lowest fractal dimension with a value of 2.29 compared to 2.36 and 2.42 for Jet A-1 and the diesel produced particulate emissions respectively at the NL engine power setting. A reduction in the fractal dimension is observed with respect to the engine operating condition as the fractal dimension for the PM emissions for Jet A-1 at the BL engine power setting is 2.30 compared to 2.36 at the NL engine power setting.

The implication of the observed fractal is that the particle structure of identical diameters for the PM emission from the fuels at burnt at the NL engine power conditions are different

and therein lies the rationale for the observed variation in densities detailed in Table 3. A higher fractal dimension suggests that the individual particles that make up the PM emissions contain more spaces. Thus, the higher fractal dimension observed for Diesel particle emissions shows that its individual particles contain more spaces compared to identical particles of Jet A-1 and Banner Solvent generated PM emission. Meanwhile, Diesel contains a wider spectrum of hydrocarbons including heavier hydrocarbons compared to Jet A-1 and Banner Solvent and expectedly produces more volatile species as a result of incomplete combustion. The volatile species which transform with time to CPM, adsorb or condense on the solid PM fractions thus filling up (Johnson et al., 2015) the spaces in the solid
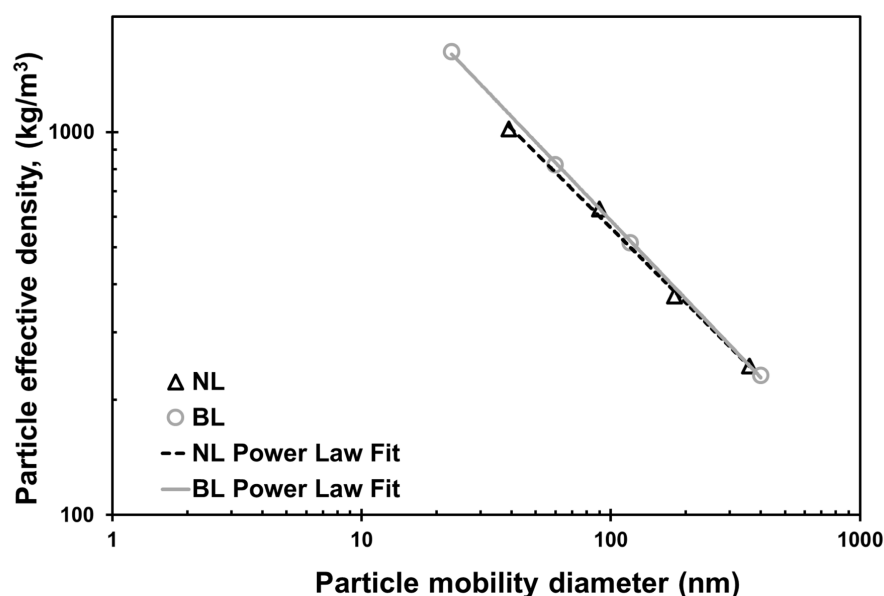


**Fig. 4 – Power law trend lines of effective densities against the mobility diameter for Jet A-1 at the NL and BL conditions respectively. NL: no load; BL: bleed load.**

**Table 3 – Results of effective densities of the same particle sizes for diesel and banner solvent.**

| Size (nm) | Density (kg/m$^3$) | |
|---|---|---|
| | Diesel | Banner solvent |
| 30 | 1181.28 | 1259.09 |
| 150 | 475.91 | 437.99 |
| 200 | 387.94 | 358.10 |

**Table 4 – Power law functions for all the test points including the overall functions for the test fuels at NL and the overall function for Jet A-1 at NL and BL.**

| Fuel | Engine power setting | Power law fit |
|---|---|---|
| Banner solvent (kg/m$^3$) | NL | $\rho_{eff} = 0.006 d_m^{(2.29 - 3)}$ |
| Jet A-1 (kg/m$^3$) | NL | $\rho_{eff} = 0.0210 d_m^{(2.36 - 3)}$ |
| Diesel (kg/m$^3$) | NL | $\rho_{eff} = 0.0480 d_m^{(2.42 - 3)}$ |
| Jet A-1(kg/m$^3$) | BL | $\rho_{eff} = 0.0078 d_m^{(2.30 - 3)}$ |

particles and not growing the particle size. The result is an increased mass of the particle and an unchanged volume. Consequently, the observed high particle density for individual particle sizes of 150 and 200 nm from diesel compared to Banner Solvent generated particulate matter suggest that the voids are filled up with condensed PM. In contrast, the lower particle density observed for the 30 nm of the diesel PM suggests that the voids, unlike the larger particles, are not filled. This is possibly because the larger particles have larger surface area to attract the condensation of the volatile particulate matter.

In a similar experiment conducted by Durdina et al. (2014), effective density was measured against mobility diameter for emissions from a commercial turbofan engine burning conventional Jet A-1. Three test conditions were tested at different thrust levels (3%–5%, 15%–30%, 50%–100%). The power laws found in this study are compared against the results obtained by Durdina et al. (2014) in Fig. 5. The respective power laws for each fuel have been truncated based on the predominant mobility diameters reported by the DMS500 results presented in Fig. 2 and the ranges reported by Durdina et al. (2014).

The difference in operating conditions and design purpose of an APU and a propulsive turbofan do not provide a like for like comparison for these results. A comparison is illustrative however, as to the significance of varying fuel composition compared to variable thrust for the same fuel. Nonetheless, as this configuration has not previously been tested using an APU, this work by Durdina et al. (2014) provides the closest results in the public domain for comparison. The variations in $D_m$, the mass mobility exponent and k, the mass mobility prefactor between this work and that of Durdina et al. (2014) is shown in Table 5.

As expected, both combustion platforms show a decrease in effective density with increasing particle size due to the common feature of agglomeration and an increased fractal geometry at larger diameters. The fundamental operative difference between an APU and propulsive Gas Turbine is apparent when comparing the largest diameter of particle emitted. As hypothesized by Durdina et al. (2014), a variation in thrust causes different residence times for combustion to take place, resulting in incomplete combustion and reduced oxidation leading to larger primary particle diameters with a higher fractal dimension. This is apparent when comparing the mass mobility exponent of the 50%–100% condition in Table 5 (2.635) with lower thrust conditions (2.37 and 2.5). APU operation facilitates similar residence times and as a result, the predominant range of particle sizes (Fig. 2) is comparable (20–250 nm) with the exception of
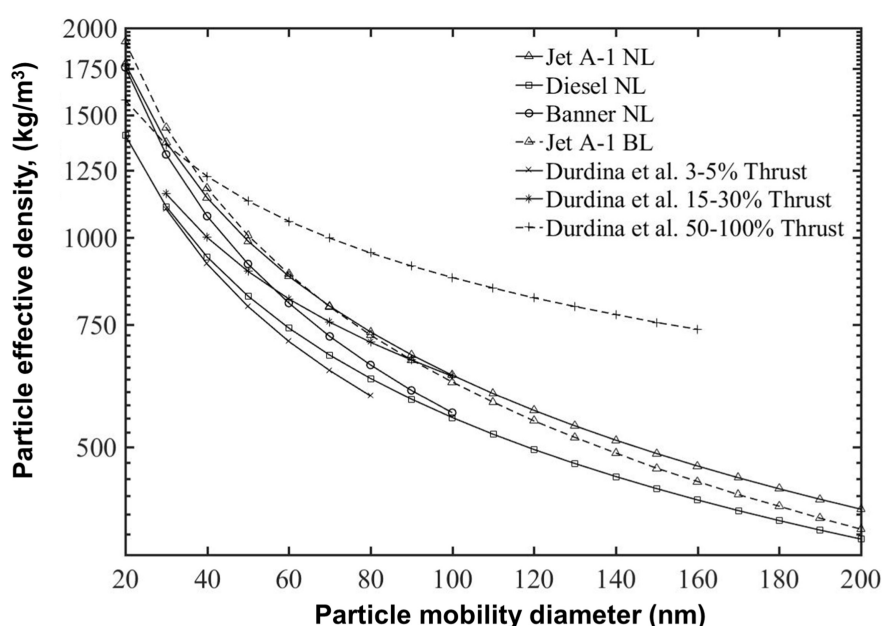


**Fig. 5 – Comparison of power laws derived in this study for fuel variation in an APU with thrust variation found by Durdina et al. (2014). APU: Auxiliary Power Unit.**

| Coefficient | Jet A-1 NL | Banner Solvent NL | Diesel NL | Jet A-1 BL | Jet A-1 3%–5% thrust | Jet A-1 15%–30% thrust | Jet A-1 50%–100% thrust |
|---|---|---|---|---|---|---|---|
| $D_m$ | 0.0210 | 0.006 | 0.0480 | 0.0078 | 0.0200 | 0.200 | 2.44 |
| $k$ | 2.36 | 2.29 | 2.42 | 2.30 | 2.37 | 2.5 | 2.635 |

Table 5 – Comparison of the power law coefficients found derived in this work for Jet A-1, Banner Solvent and Diesel with those reported by Durdina et al. (2014) for Jet A-1 at varying thrust levels.

Banner NP 1014. This is most likely due to the absence of any aromatic content in NP 1014 and its reduced ability to form Polycyclic Aromatic Hydrocarbons.

While variations in thrust appear to have a substantial effect on particle density, the effect of fuel variation is not insignificant. At 80 nm (The largest size observed for every fuel and thrust condition), thrust dependent particle density varies by − 16.3% and 34.4% (compared to 15%–30% thrust). At 80 nm for APU fuel variation, density varies by − 14.3% (Diesel NL) and − 10.3% (Banner NP 1014) compared to Jet A-1 NL.

## 3. Conclusions

As a result of this study, the effective density and the fractal dimension particles emitted from a gas turbine combustor were determined for a particle size range of around 30–450 nm. The effective density was found to decrease with increase in particle size. The fuel burnt and engine operating condition affect the effective density and the fractal dimension values of the particles. Thus, a single value cannot be used for these parameters to determine the mass concentration from the number size distribution measurement of the PM emission for the combustion of different fuels for a gas turbine engine.

## REFERENCES

Abegglen, M., Durdina, L., Brem, B.T., Wang, J., Rindlisbacher, J.C., Corbin, J.C., et al., 2015. Effective density and mass–mobility exponents of particulate matter in aircraft turbine exhaust: dependence on engine thrust and particle size. J. Aerosol Sci. 88, 135–147.

Anderson, B.E., Branham, H.S., Hudgins, C.H., Plant, J.V., BAllenthin, J.O., Miller, T.M., et al., 2005. Experiment to characterize aircraft volatile aerosol and trace-species emissions (EXCAVATE). National Aeronautics and Space Administration. Report (NASA/TM-2005-213783).

Automotive Fuels-Diesel Requirements and Test Methods. CEN, Brussels.

Corporan, E., Quick, A., DeWitt, M.J., 2008. Characterization of particulate matter and gaseous emissions of a C-130H aircraft. J. Air Waste Manage. Assoc. 58 (4), 474–483.

DeCarlo, P.F., Slowik, J.G., Worsnop, D.R., Davidovitz, P., Jimenez, J.L., 2004. Particle morphology and density characterization by combined mobility and aerodynamic diameter measurements. Part 1: theory. Aerosol Sci. Technol. 38 (12), 1185–1205.

Durdina, L., Brem, B.T., Abegglen, M., Lobo, P., Rindlisbacher, T., Thompson, et al., 2014. Determination of PM mass emissions from an aircraft turbine engine using particle effective density. Atmos. Environ. 99, 500–507.

Ehara, K., Hagwood, C., Coakley, K.J., 1996. Novel method to classify aerosol particles according to their mass-to-charge ratio—aerosol particle mass analyser. J. Aerosol Sci. 27 (2), 217–234.

Hagen, D., Whitefield, P., Paladino, J., Trueblood, M., Lilenfield, H., 1998. Particulate sizing and emission indices for a jet engine exhaust sampled at cruise. Geophys. Res. Lett. 25 (10), 1681–1684.

Johnson, T.J., Olfert, J.S., Symonds, J.P.R., Johnson, M., Rindlinsbacher, T., Swanson, J.J., et al., 2015. Effective density and mass-mobility exponent of aircraft turbine particulate matter. J. Propuls. Power 31 (2), 573–582.

Kelly, W.P., McMurry, P.H., 1992. Measurement of particle density by inertial classification of differential mobility analyzer–generated monodisperse aerosols. Aerosol Sci. Technol. 17 (3), 199–212.

Khandelwal, B., Ubogu, E., Akram, M., Blakey, S., Wilson, C.W., 2013. Experimental analysis on emission production and performance of stressed 100% SPK, stressed fully formulated synthetic jet fuel and Jet A-1 in a small gas turbine engine. Proceedings of the 11th International Energy Conversion Engineering Conference, San Jose, CA, USA, pp. 14–17.

Kinsey, J.S., Dong, Y., Williams, D.C., Logan, R., 2010. Physical characterization of the fine particle emissions from commercial aircraft engines during the Aircraft Particle Emissions eXperiment (APEX) 1–3. Atmos. Environ. 44 (17), 2147–2156.

Kinsey, J.S., Timko, M.T., Herndon, S.C., Wood, E.C., Yu, Z., Miake-Lye, R.C., et al., 2012. Determination of the emissions from an aircraft auxiliary power unit (APU) during the Alternative Aviation Fuel Experiment (AAFEX). J. Air Waste Manage. Assoc. 62 (4), 420–430.

Li, Y., Xue, J., Johnson, K., Durbin, T., Villela, M., Pham, L., Hosseini, S., et al., 2014. Determination of suspended exhaust PM mass for light-duty vehicles. SAE Technical Paper 2014-01-1594.

Li-Jones, X., Penko, P.F., Moses, C., 2007. Gaseous and particle emissions in the exhaust of a T700 helicopter engine. ASME Turbo Expo: Power for Land, Sea, and Air, pp. 395–411.

Lobo, P., Hagen, D.E., Whitefield, P.D., 2011. Comparison of PM emissions from a commercial jet engine burning conventional, biomass, and Fischer–Tropsch fuels. Environ. Sci. Technol. 45 (24), 10744–10749.

Lobo, P., Christie, S., Khandelwal, B., Blakey, S.G., Raper, D.W., 2015. Evaluation of non-volatile particulate matter emission characteristics of an aircraft auxiliary power unit with varying alternative jet fuel blend ratios. Energy Fuel 29 (11), 7705–7711.

McMurry, P.H., Wang, X., Park, K., Ehara, K., 2002. The relationship between mass and mobility for atmospheric particles: a new technique for measuring particle density. Aerosol Sci. Technol. 36 (2), 227–238.

Olfert, J.S., Collings, N., 2005. New method for particle mass classification—the Couette centrifugal particle mass analyzer. J. Aerosol Sci. 36 (11), 1338–1352.

Onasch, T.B., Jayne, J.T., Herndon, S., Worsnop, D.R., Miake-Lye, R.C., Mortimer, P., Anderson, B.E., 2009. Chemical properties of aircraft engine particulate exhaust emissions. J. Propuls. Power 25 (5), 1121–1137.

Park, K., Kittelson, D.B., McMurry, P.H., 2004. Structural properties of diesel exhaust particles measured by transmission electron microscopy (TEM): relationships to particle mass and mobility. Aerosol Sci. Technol. 38 (9), 881–889.

Petzold, A., Marsh, R., Johnson, M., Miller, M., Sevenco, Y., Delhaye, D., et al., 2011. Evaluation of methods for measuring particulate matter emissions from gas turbines. Environ. Sci. Technol. 45 (8), 3562–3568.

Procedure for the Continuous Sampling and Measurement of Non-Volatile Particle Emissions from Aircraft Turbine Engines. SAE Aerospace, SAE International, Warrendale.

Roy, S., Khandelwal, B., 2015. Comparison of gaseous emissions between Jet A-1 and severely hydro-processed jet fuel from conventional sources. 13th International Energy Conversion Engineering Conference. American Institute of Aeronautics and Astronautics.

Symonds, J.P., Reavell, K.S.J., Olfert, J.S., Campbell, B.W., Swift, S.J., 2007. Diesel soot mass calculation in real-time with a differential mobility spectrometer. J. Aerosol Sci. 38 (1), 52–68.

Timko, M.T., Yu, Z., Onasch, T.B., Wong, H.W., Miake-Lye, R.C., Beyersdorff, A.J., et al., 2010. Particulate emissions of gas turbine engine combustion of a Fischer–Tropsch synthetic fuel. Energy Fuel 24 (11), 5883–5896.

Vander Wal, R.L., Bryg, V.M., Huang, C.H., 2014. Aircraft engine particulate matter: macro- micro- and nanostructure by HRTEM and chemistry by XPS. Combust. Flame 161 (2), 602–611.